Journal of Quantitative Spectroscopy & Radiative Transfer 241 (2020) 106720

Contents lists available at ScienceDirect

Journal of Quantitative Spectroscopy & Radiative Transfer

journal homepage: www.elsevier.com/locate/jqsrt

Minimum principles in electromagnetic scattering by small aspherical particles: Extension to differential cross-sections

Alexander B. Kostinski [a], Yevgeny Derimian [b,*]

[a] Department of Physics, Michigan Technological University, 1400 Townsend Drive, Houghton, MI 49931, USA
[b] Univ. Lille, CNRS, UMR 8518 - LOA - Laboratoire d'Optique Atmospherique, Lille F-59000, France

ARTICLE INFO

Article history:
Received 21 June 2019
Revised 14 October 2019
Accepted 23 October 2019
Available online 24 October 2019

Keywords:
Electromagnetic scattering
Particle shape
Extinction

ABSTRACT

In this work we extend earlier findings that optically small and randomly oriented ovaloids extinguish more radiation than equal volume spheres [1], to differential cross-sections. Rather than working with the normalized phase function as is typically done in radiative transfer and in remote sensing, we compute absolute *un-normalized* differential scattering cross-sections $C_{scatt}(\theta)$ and show that for optically small to moderate size parameters, not only does the integrated extinction by randomly oriented spheroids $C_{ext}(\theta)$ exceed that of equal volume spheres but it does so at each scattering angle (θ). Furthermore, at each θ, the effect is monotonic with the aspect ratio (AR) and its magnitude is appreciable for realistic refraction indices of terrestrial aerosols. Spherical shape optimality holds for absorption cross-sections as well. Absorption is not only volume-dependent but increases substantially with asphericity, rising by two orders of magnitude near resonant lines. We also compare the asymmetry parameter (g) and single scattering albedo (ω_0) of randomly oriented spheroids to that of equal volume spheres and find that while the dependence of the ratios on the axis ratio is monotonic, change of either sign is possible, depending on the index of refraction. Ice in the microwave and quartz in the thermal IR are used to illustrate applications in atmospheric remote sensing.

1. Introduction

In an earlier work in this journal we reported that optically small-to-moderate and randomly oriented ovaloids extinguish more radiation than equal volume spheres [1]. The plausibility of this result was argued on purely geometrical grounds, via the isoperimetric property of the sphere (least area at a given volume). This can be illustrated by a spheroidal surface area, normalized by that of an equal volume sphere (denoted S_r), regarded as a function of the aspect ratio [1]. Such scaled surface area is given by

$$S_r = (1/2)\left(1-e^2\right)^{-1/3} + (1/4e)\left(1-e^2\right)^{2/3} ln[(1+e)/(1-e)] \tag{1}$$

where $e^2 \equiv 1-(c/a)^2$ for oblate spheroids, and

$$S_r = (1/2)\left(1-e^2\right)^{1/3} + (1/2e)\left(1-e^2\right)^{-1/6} \sin^{-1}(e) \tag{2}$$

with $e^2 \equiv 1-(b/a)^2$ for prolate spheroids. Both functions are monotonic and smooth, with a minimum at the spherical value of $e = 1$.

In [1], we argued that although extinction by the optically small particle (low frequency or Rayleigh) is rooted in electrostatics, geometry still causes, for a given particle volume, the least orientation-average dipole moment to occur for the spherical surface. We refer the reader to [1–5] for the relevant literature survey and pose here the follow-up question: How do randomly-oriented optically small to moderately sized spheroids compare to equal volume spheres with regards to the *angular* distribution of scattering, that is, *differential* scattering cross-sections? For the sake of clarity we shall confine the discussion and calculation to the case of *unpolarized* radiation throughout this paper. This question of non-spherical shape and its impact on scattering is, of course, not new and has been explored by many researchers, e.g., [6–8] but our constraints are somewhat different.

2. Optimality of the spherical shape holds for all directions when suitably compared

One might reasonably expect the answer to the question just posed above to be intricately angle-dependent. Indeed, spheroidal

* Corresponding author.
E-mail addresses: kostinsk@mtu.edu (A.B. Kostinski), yevgeny.derimian@univ-lille.fr (Y. Derimian).

https://doi.org/10.1016/j.jqsrt.2019.106720

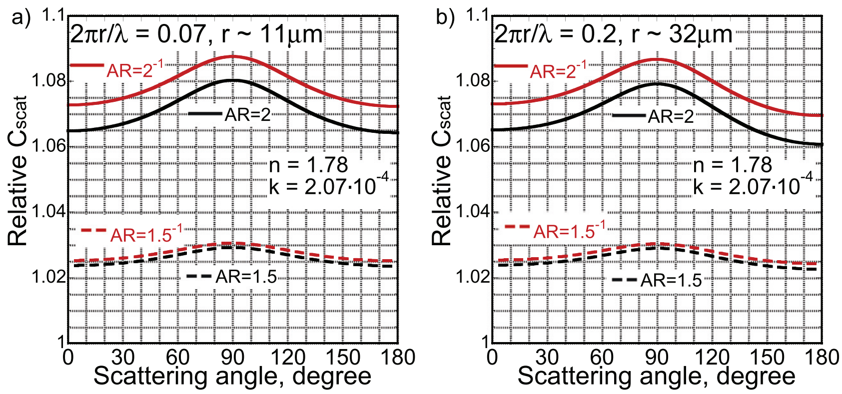

Fig. 1. Relative differential scattering cross-section of randomly oriented spheroids, normalized by those of equal volume sphere. The real ($n = 1.78$) and imaginary ($k = 2.07 \times 10^{-4}$) parts of the refractive index are for ice at $\lambda = 1$ mm. These curves show that optically small spheroids scatter more than equal volume spheres [1] not only in total but also for each scattering direction: e.g., see panel (a) where all curves are above unity. Panel (b) is size beyond the Rayleigh region. As the particle asphericity increases, the effect becomes monotonically more pronounced at all angles. These results may appear to counter many of the literature reports that size-distributed spheroid mixtures scatter more than spheres at some angles but not others, e.g., Fig. 3, p. D11208 of [6]. However, there is no discrepancy as our results are for the absolute (un-normalized) *differential* cross-sections of optically small to moderately-sized particles.

models have been studied thoroughly e.g., [6–8] and intricate patterns have been reported as comparative phase function plots, e.g., the phase matrix element P_{11} vs. the scattering angle diagrams. Division by the total cross-section normalizes the traditional phase function to unity which is eminently reasonable, given the probability interpretation, i.e., a photon has to scatter somewhere. Furthermore, given practical remote sensing constrains on retrievals, working with the normalized phase function is convenient. Note, however, that our question is about the direct problem of comparing *absolute* scattering intensities of randomly oriented particles of the same volume but of different shapes. In order to properly enforce the equal volume constraint, one must adhere to the differential scattering cross-section interpretation, implying that the integral over all angles must add up to the total cross-section. But, at a fixed volume, the total cross-section attains minimum for the spherical shape as was shown in the earlier paper [1]. Therefore, for proper comparison, for each shape the integral of the *unnormalized* phase function over all solid angles must add up to the total cross-section for *that* shape.

Because earlier work [1] showed that, given the same volume, the spheroids scatter more than spheres in total, the question can be rephrased as: how is the spherical deficit distributed over all directions? Calculations presented here show that optically small to moderate spheroids scatter more than spheres not just in total but *for all angles individually*. Furthermore, the angular spherical deficit increases monotonically with increasing asphericity at all angles.

To compute the differential cross-sections for small to moderate size parameters $x = 2\pi r/\lambda$ (r is the radius of equal-volume sphere), we used the T-matrix method, adapted for oblate and prolate spheroids. This computational technique, conceived by Waterman and developed by Mishchenko is also known as the extended boundary technique method (EBCM), e.g. [7]. Specifically, the computations were conducted using a code created for simulation of optical properties of non-spherical particles [6] using the updated version [9,10], which provides an exact solution for electromagnetic scattering by randomly oriented spheroids. For internal consistency checks, the calculations for spheres were conducted using the same T-matrix code, but setting the axis ratio to one.

We begin with the typical dielectric values (n denotes the real and k the imaginary part of the refractive index, respectively) characteristic of cloud ice particles in the microwave region (1 mm), e.g., [11], pp.167-9. Fig. 1 shows the relative scattering cross-section C_{scatt} vs. the scattering angle θ (panels a and b). The adjective "relative" throughout this paper refers to the ratio of the relevant quantity for randomly oriented spheroids to that of an equal-volume sphere. Thus, relative C_{scatt}, exceeding unity is indicative of spheroids scattering more than spheres at that particular angle. The axis ratio AR for spheroids is defined as $AR \equiv a/b$ where a and b are the axis of rotational symmetry and axis, normal to the axis of rotational symmetry, respectively. Recall that an prolate spheroid is generated by rotating ellipse about its major axis (a) whereas in the oblate case the ellipse is rotated about the minor axis (still a).

While Fig. 1 gives an impression that the asphericity effect is small, it is not so for many ubiquitous refraction indices, e.g., those typical of quartz in the thermal infrared (TIR). This is illustrated in Fig. 2 where in addition to the curve for ice, the quartz calculations are shown. Note that the quartz is birefringent and we use the refraction data for the extraordinary quartz (quartz E, for short) [12] merely for illustrative purposes. The two panels of Fig. 2 correspond to the two size parameters (small and moderate) and demonstrate the large magnitude of the effect for the TIR indices of quartz [13]. The axial ratio is kept at the relatively modest value of 2 but its effect in TIR exceeds a factor of 3. The conclusion holds for both size parameters. Furthermore, we note that, compared to the Rayleigh regime ($x = 0.07$), the spheroidal access in scattering at $x = 0.2$ (panel b) is more pronounced so implications of asphericity for remote sensing can be significant. This is illustrated with the sizes of 0.1 and 0.3 microns, representing the fine mode aerosol particles, present in mineral dust and affecting aerosol optical characteristics in TIR, e.g, [14], see p. 238.

In order to extend our findings to total extinction we now turn to absorption. The frequently made statement that absorption depends only on volume is not accurate. For example, absorption depends on how the total suspension volume is dispersed (i.e., distributed in particle size), that is it depends on the size distribution of particles, particularly for broad distributions, e.g., see [15]. Similarly, at a given volume, the absorption amount depends on particle shape. Even the sign of the effect depends on material properties and was the subject of some debate, e.g., see [16] and [8] concerning dielectric vs. ionic optically small ellipsoidal particles. Therefore, we extend the calculations to optically moderate sizes and three different refraction regions in order to explore the interplay between asphericity and material properties.

As in Fig. 2, our three illustrative examples are for ice in the microwave (1 mm) and quartz E in the TIR at 8.86 μm and at 9.33 μm, bracketing the quartz E resonance line as explored in prior work on modeling dust properties, [14], p. 231, Fig. 2 therein, panel d). The real and imaginary parts of the refractive index for the three λs

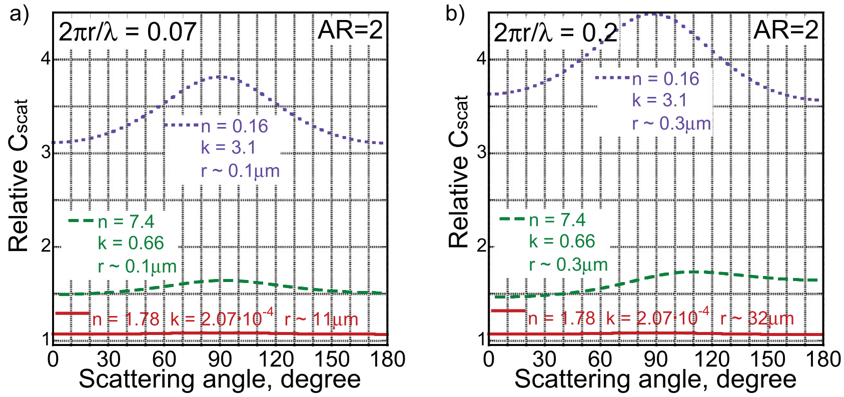

Fig. 2. Relative differential scattering cross-section for ice and quartz. Plot of the relative differential scattering cross-section C_{scatt} as in Fig. 1 but contrasting material refraction. The axis ratio kept at 2. Panels (a) and (b) have the size parameters of $x \equiv 2\pi r/\lambda = 0.07$ and 0.2, respectively. The real (n) and imaginary (k) parts of the three refractive indices are shown in the legends and are as follows: $n = 1.78$ and $k = 2.07 \times 10^{-4}$ at $\lambda = 1$ mm (ice), $n = 0.16$ and $k = 3.1$ at 8.86 microns and $n = 7.4$ and $k = 0.66$ at 9.33 microns (quartz E). In the thermal IR, impact of asphericity extends to $> 300\%$.

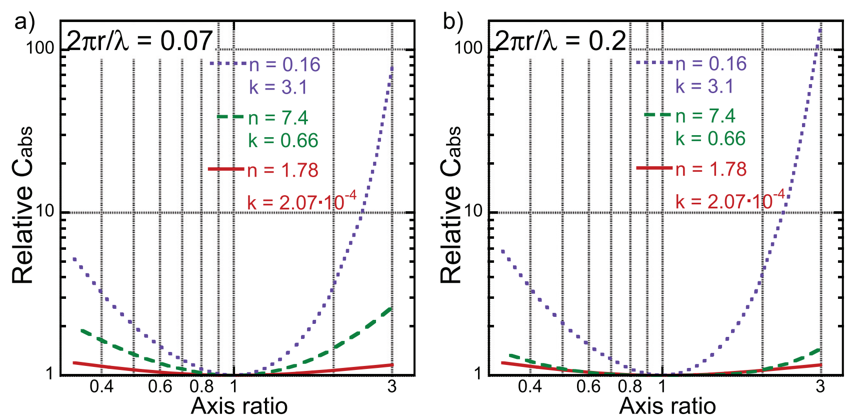

Fig. 3. Relative absorption cross-section versus the axis ratio for the three different sets of material properties. The magnitude of the aspericity effect for the dotted violet curve in the thermal IR is several hundred percent. For the prolate spheroids of axis ratio of 3, asphericity deficit increases from a factor of 80 to beyond 100 as the size parameter changes to 0.2 (panel b).

are: $n = 1.78$, $k = 2.07 \times 10^{-4}$; $n = 0.16$, $k = 3.1$, $n = 7.4$, $k = 0.66$, respectively.

Fig. 3 shows that the asphericity-caused increase is monotonic with the aspect ratio for both size parameters and extends beyond the Rayleigh region (panel b). Evidently, absorption and extinction do not depend solely on particle volume. Furthermore, not only is the asphericity important but it can be dominant, e.g. going from a factor of 60 to beyond 100 for the axial ratio of 3 as the size parameter changes from 0.07 to 0.2. Thus, the impact of asphericity is sensitive to the index of refraction changes near resonances as in the TIR sensing of aerosols.

The optical depth τ depends linearly on the extinction cross-section and, hence, on asphericity. In order to gain an intuitive appreciation for the broader effect of asphericity on climatic radiative transfer, we turn to the two variables arising in a self-similar solution: e.g., in the expressions for, say, scaled optical depth $(1-g)\tau$ and semi-infinite medium albedo, e.g, see [17] and also [18,19]. These are the asymmetry parameter g, defined as the average cosine of the scattering angle, weighted by the phase function $P(\theta)$ [17,20]

$$g \equiv \langle \cos(\theta) \rangle = \frac{1}{2} \int_0^{\pi} \cos\theta P(\theta) \sin\theta d\theta \tag{3}$$

and the single scattering albedo ω_0 (the ratio of scattering to total extinction, $\omega_0 \equiv \sigma_{scatt}/\sigma_{ext}$). Recall that we treat the phase functions $P(\theta)$ as the differential cross-sections in the first two figures so that they integrate out to their *respective* total cross-sections.

Again, we define and calculate g and ω_0 in the relative sense, that is, normalized by the same quantity for the equal-volume spheres.

$$\frac{g_{spheroid}}{g_{sphere}} \equiv \frac{\langle \cos(\theta) \rangle_{spheroid}}{\langle \cos(\theta) \rangle_{sphere}}, \tag{4}$$

and

$$\omega_{0,spheroid}/\omega_{0,sphere} \equiv \frac{\sigma_{scatt,sphere}}{\sigma_{scatt,spheroid}} / \frac{\sigma_{ext,sphere}}{\sigma_{ext,spheroid}} \tag{5}$$

The results are shown in Figs. 4 and 5 versus the aspect ratio. Consider the optically small particle (the Rayleigh region) shown in panel (a) of Fig. 4. For the red curve (i), representative of conventional dielectric refraction, the *absolute* asymmetry is small ($g \sim 10^{-3}$) and not shown but remains positive (slightly more scattering forward) while the relative asymmetry (left panel) of the spheroids is above unity. The absolute asymmetry is still small in case of size parameter of 0.2 but increases to almost $g \sim 10^{-2}$ and again remains positive (preference for scattering forward) while the relative asymmetry (right panel) of the spheroids is above unity. This means that randomly oriented spheroids scatter proportionally more forward than do equal volume spheres, the excess over the spherical value increasing monotonically as AR increases. The situation is different in the case (ii) of the dashed green curve, representing the thermal infrared: the absolute asymmetry is still small: $g \sim 10^{-3}$, (left panel) and $g \sim 10^{-2}$ (right panel), and positive but the relative asymmetry is below unity: spheroids scatter forward less than the spheres. Case (iii) of the dotted violet curve

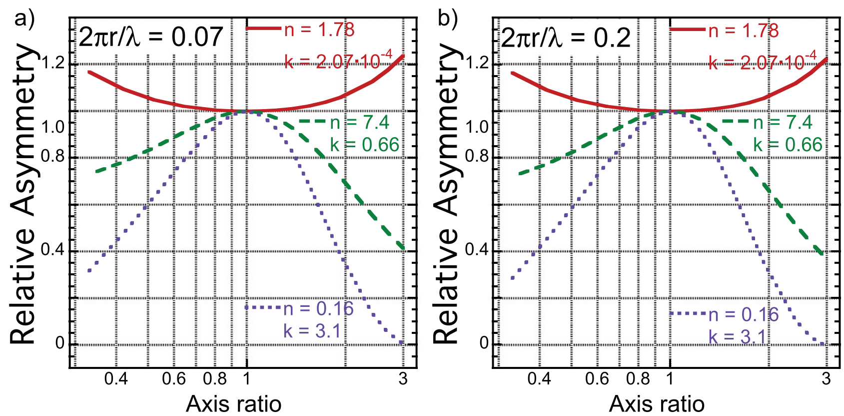

Fig. 4. Relative asymmetry parameter g_{rel} versus the axis ratio (AR) for the three different sets of material properties. a) Rayleigh region of optically small particles. As expected, symmetric phase functions yield $g = 0$ and relative $g = 1$ at AR = 1. The monotonic increase in g_{rel} with AR is also evident as well as the sign change of $g_{rel} - 1$ between the ice/microwaves and the quartz in TIR. In contrast to the microwave scattering by ice, in TIR optically small as well as moderate (panel b) quartz ovaloids scatter more towards the backward hemisphere than do equal volume spheres as detailed in text. The calculated patterns are robust in the optically small-to-moderate size region and hardly any change is discernible as size parameter changes from 0.07 to 0.2.

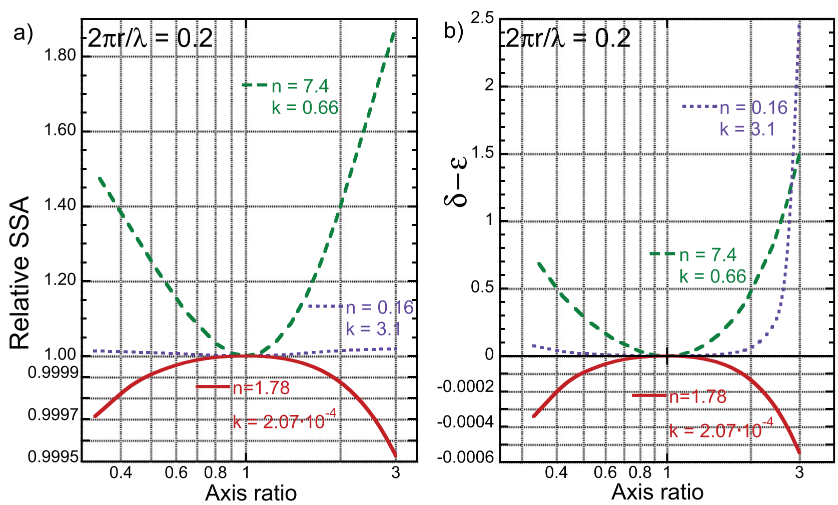

Fig. 5. Relative Single Scattering Albedo ω_0 versus the axis ratio for the three different sets of material properties. Only results for the size parameter 0.2 are shown because ω_0 is exceedingly small for the size parameter of 0.07 as absorption dominates scattering in this case. Right panel explores $(\omega_0 - 1)$ as detailed in text.

(thermal infrared at slightly higher than the resonant frequency) is different yet: the absolute asymmetry (not shown) is near zero but switches sign: spheroids and spheres scatter more backwards, reminiscent of the magnetic dipole pattern [21]. To that end, we remark that the recently discovered importance of the magnetic dipole moment in the scattering by optically small purely dielectric particles, [22] remains unexplored in atmospheric physics. Returning to case (iii) of Fig. 4, the relative asymmetry is below unity so that spheres scatter a larger fraction of radiation backward than do equal volume random collections of spheroids. The pattern of the three cases persists in panel b), despite a 3-fold increase in the size parameter.

The same three cases are examined in Fig. 5 with respect to the single scattering albedo (SSA, ω_0). It is seen that the *relative* ω_0 flips from a maximum to a minimum at the spherical shape, depending on the optical properties. The absolute values of ω_0 are not shown in the figure but vary as follows from spherical to maximal spheroidal value: 0.918 to 0.917 for the red curve; 0.143 to 0.269 for the green curve; 0.162 to 0.165 for the violet curve. Note that the quantitatively significant differences in SSA vs. the axis ratio occur, for the size parameter of 0.2, in the TIR regime where SSA is only about 15% to 20% so that total extinction is still dominated by absorption.

Why does the relative single scattering albedo switch from the spherical maximum in the microwave to the minimum in the thermal infrared? Spheroids exceed equal-volume spheres in scattering as well as in absorption so when it comes to a ratio, this flip is a result of a competition of the two effects. The right panel of Fig. 5 examines this competition via a simple perturbation argument applied to Eq. (5). For optically small to moderately-sized particles, $\sigma_{scatt} << \sigma_{ext}$ so that the numerator and the denominator in the above equation are both slightly larger than unity and monotonic. Therefore, the relative ω_0 can be expanded as $\omega_{0,spheroid}/\omega_{0,sphere} \equiv (1+\delta)/(1+\epsilon) \approx 1 + (\delta - \epsilon)$. The latter expression is plotted vs. the axis ratio in the right panel of Fig. 5. Hence, in thermal IR, for moderately small spheroids, the asphericity impact on scattering (δ) overtakes that of absorption (ϵ), rendering the spherical value a minimum.

3. Concluding remarks

This work extends earlier findings that randomly oriented, optically small to moderately-sized spheroids extinguish more radiation than equal volume spheres [1], to differential cross-sections. Rather than working with the normalized phase function, we computed absolute (un-normalized) differential scattering cross-sections $C_{scatt}(\theta)$ and showed that for optically small to moderate size parameters, not only does the extinction by randomly oriented spheroids $C_{ext}(\theta)$ exceed that of equal volume spheres in total but at each scattering angle (θ) as well. Additionally, the effect is monotonic with the aspect ratio and its magnitude is appreciable for terrestrial aerosols in TIR.

Bounds on optimal shapes can be useful, e.g., in the geometrical optics limit (optically large particles) twice the geometric cross-section is a good approximation to the total extinction cross-section. When this is used with the Cauchy theorem that orientation-averaged cross-sectional area of an ovaloid equals 1/4 of its surface area, the geometrical limit implies that spherical total cross-sections are the least for any randomly oriented convex particles of equal volume [23]. In absolute terms, whether optically large or small, convex aspherical particles extinguish more energy than their equal-volume spherical counterparts. This is also true for scattering in a differential sense. Furthermore, the effect, for some materials, be an order of magnitude even for a rather modest axis ratio of 2.

Realistic situations usually involve a distribution of aerosol sizes and broadband radiation. To that end, it would be useful to extend our considerations to a range of sizes or wavelengths. Let us, therefore, remark on spectrally integrated extinction. For spherical particles, spectrally integrated cross-section is given by ([24])

$$\int_0^\infty C_{ext}(\lambda)d\lambda = 4\pi^3 a^3 \left(\frac{\varepsilon(0)-1}{\varepsilon(0)+2}\right) \tag{6}$$

and, remarkably, it involves only the static dielectric constant, because of the Kramers–Kronig relations. For randomly oriented ellipsoidal particles, the integrated extinction has the same form as eqn. (6) but with the pre-factor which depends on the three depolarization factors [25], L_is. Specifically, using the non-magnetic case in Eqs. (2.11) and (4.1) of [25] the relative integrated extinction of spheroids (the integrated extinction of spheroid divided by that of sphere) can be written as

$$\int_0^\infty \bar{C}_{ext}(\lambda)d\lambda|_{rel} = \frac{\left(\frac{1}{1+\chi L_1} + \frac{1}{1+\chi L_2} + \frac{1}{1+\chi L_3}\right)}{\frac{3}{1+\chi/3}}. \tag{7}$$

where the over-bar signifies orientation averaging and χ is the susceptibility. This expression is identical to the expression for relative orientation-averaged polarizability and the right-hand-side always exceeds unity with the minimum at the spherical value [1]. Thus, the extinction, integrated over all frequencies, for an ellipsoidal particle exceeds that of an equal-volume sphere.

Of course, at some size parameters, near certain Mie resonances, in particular, the relative extinction can drop below unity and the spheres optimality may not hold (Fig. 4 in [1]). In realistic atmospheric applications, where averaging over particles size and aspect ratio is required, such dips induce variations of the spectral characteristics, e.g., see (Fig. 8 in [26]) but the shape effect remains pronounced for the integrated optical characteristics [26] as would be suggested by the frequency-integrated results above.

The magnitude of the absorption dependence on particle shape is shown to depend rather sensitively on complex refractive index near the resonances. Although frequently neglected, the absorption dependence on particle shape is seen to be important for airborne mineral dust observations in TIR.

We conclude with a few remarks concerning the random orientation assumption. Settling dust particles in a relatively calm air (laminar flow) orient preferentially, experience greater drag and stay aloft longer, e.g., see [27]. This is also true for ice crystals and glints from such horizontally oriented tiny mirrors have recently been detected a million miles away [28,29]. Nevertheless, even in such cases the random orientation perspective can yield useful results. Indeed, most aerosols, although aspherical, are irregularly shaped. Suspensions of such irregularly shaped particles can be represented by a collection of particles whose polarizability and resistence tensors are multiples of unity, e.g., [30]. For example, a cube has a settling speed (and EM dipole moment) independent of orientation. Thus, the cube's low frequency electromagnetic and aerodynamic responses are independent of orientation and, alternatively, of incident direction and polarization. In addition to platonic solids, [1], the set of such shapes includes any particles with three mutually orthogonal axes of symmetry, e.g., truncated cubes, Archimedean solids, mutually perpendicular wire triplets (jacs), etc.

Declaration of Competing Interest

The authors declare that they have no known competing financial interests or personal relationships that could have appeared to influence the work reported in this paper.

Acknowledgements

This work was supported by the NSF grant AGS-1639868 and by the CaPPA project (Chemical and Physical Properties of the Atmosphere), funded by the French National Research Agency through the Programme d'Investissement d'Avenir under contract "ANR-11-LABX-0005-01" and by the Regional Council Nord Pas de Calais - Picardie and the European Funds for Regional Economic Development. The computational assistance of Dr. T. Lapyonok with a variant of the T-matrix method is gratefully acknowledged. We are grateful to two anonymous reviewers for insightful comments.

Supplementary material

Supplementary material associated with this article can be found, in the online version, at doi:10.1016/j.jqsrt.2019.106720.

References

[1] Kostinski AB, Mongkolsittisilp A. Minimum principles in electromagnetic scattering by small aspherical particles. J Quant Spectrosc RadiatTransfer 2013;131:194–201. doi:10.1016/j.jqsrt.2013.08.006.
[2] Pólya G, Szegő G. Isoperimetric inequalities in mathematical physics. Annals of mathematics studies. Princeton University Press; 1951. ISBN 9780691079882.
[3] Garboczi EJ, Douglas JF. Intrinsic conductivity of objects having arbitrary shape and conductivity. Phys Rev E 1996;53:6169–80.
[4] Kang H, Milton GW. Solutions to the pólya–szegö conjecture and the weak eshelby conjecture. Arch Ratio Mech Anal 2008;188(1):93–116. doi:10.1007/s00205-007-0087-z.
[5] Jones DS. Low-frequency electromagnetic-radiation. J Inst MathAppl 1979;23(4):421–47.
[6] Dubovik O, Sinyuk A, Lapyonok T, Holben BN, Mishchenko M, Yang P, et al. Application of spheroid models to account for aerosol particle nonsphericity in remote sensing of desert dust. J Geophys Res Atmos 2006;111(D11). doi:10.1029/2005jd006619.
[7] Mishchenko M, Hovenier J, Travis L. Light scattering by nonspherical particles: theory, measurements, and applications. Elsevier Science; 1999. ISBN 9780080510200.
[8] Bohren CF, Huffman DR. Absorption cross-section maxima and dummytxdummy– minima in ir absorption bands of small ionic ellipsoidal particles. Appl Opt 1981;20(6):959–62.
[9] Mishchenko MI, Travis LD. T-matrix computations of light scattering by large spheroidal particles. Opt Commun 1994;109:16–21.
[10] Mishchenko MI, Travis LD, Lacis AA. Scattering, absorption, and emission of light by small Particles. Cambridge: Cambridge University Press; 2002.
[11] Ayvazyan G. Propagation of millimeter and submillimeter waves clouds. Handbook. Leningrad, Gidrometeorizdat, in Russian; 1991.
[12] Peterson JT, Weinman JA. Optical properties of quartz dust particles at infrared wavelengths. J Geophys Res 1969;74(28):6947. doi:10.1029/JC074i028p06947.
[13] Longtin DR, Shettle EP, Hummel JR, Pryce JD. A wind dependent desert aerosol model: Radiative properties. Tech. Rep.. OPTIMETRICS INC BURLINGTON MA; 1988.
[14] Legrand M, Dubovik O, Lapyonok T, Derimian Y. Accounting for particle nonsphericity in modeling of mineral dust radiative properties in the thermal infrared. J Quant Spectrosc RadiatTransfer 2014;149(0):219–40. doi:10.1016/j.jqsrt.2014.07.014.
[15] Smirnov AV, Shifrin KS. Light-absorption by a dispersed system. Colloid J USSR 1987;49(4):726–8.

[16] Senior TBA. Effect of particle shape on low frequency absorption. Appl Opt 1980;19(15):2483–5.
[17] Grant PW. A first course in atmospheric radiation. Madison WI USA: Sundog Publishing; 2004. p. 62–6.
[18] Baker M. Cloud microphysics and climate. Science 1997;276(5315):1072–8.
[19] Roberts G, Ramana M, Corrigan C, Kim D, Ramanathan V. Simultaneous observations of aerosol–cloud–albedo interactions with three stacked unmanned aerial vehicles. Proc Natl Acad Sci 2008;105(21):7370–5.
[20] Seinfeld J, Pandis S. Atmospheric chemistry and physics: from air pollution to climate change. New York: John Wiley and Sons, Inc.; 1998.
[21] Jackson JD. Classical electrodynamics. AAPT; 1999.
[22] Tribelsky MI, Geffrin JM, Litman A, Eyraud C, Moreno F. Small dielectric spheres with high refractive index as new multifunctional elements for optical devices. Sci Rep 2015;5:7. doi:10.1038/srep12288.
[23] Pollack JB, Cuzzi JN. Scattering by nonspherical particles of size comparable to a wavelength: a new semi-empirical theory and its application to tropospheric aerosols. J Atmos Sci 1980;37(4):868–81.
[24] Purcell EM. On absorption and emission of light by interstellar grains. Astrophys J 1969;158(2P1):433. doi:10.1086/150207.
[25] Sohl C, Gustafsson M, Kristensson G. Physical limitations on broadband scattering by heterogeneous obstacles. J Phys A 2007;40(36):11165.
[26] Derimian Y, Dubovik O, Huang X, Lapyonok T, Litvinov P, Kostinski AB, et al. Comprehensive tool for calculation of radiative fluxes: illustration of shortwave aerosol radiative effect sensitivities to the details in aerosol and underlying surface characteristics. Atmos Chem Phys 2016;16(9):5763–80. doi:10.5194/acp-16-5763-2016.
[27] Yang W, Marshak A, Kostinski AB, Várnai T. Shape-induced gravitational sorting of saharan dust during transatlantic voyage: evidence from caliop lidar depolarization measurements. Geophys Res Lett 2013;40(12):3281–6.
[28] Marshak A, Várnai T, Kostinski A. Terrestrial glint seen from deep space: oriented ice crystals detected from the lagrangian point. Geophys Res Lett 2017;44(10):5197–202.
[29] Várnai T, Kostinski AB, Marshak A. Deep space observations of sun glints from marine ice clouds. IEEE Geosci Remote Sens Lett 2019.
[30] Guazzelli E, Morris JF. A physical introduction to suspension dynamics, 45. Cambridge University Press; 2011.